Effects of oxygen enrichment on diesel spray flame soot formation in O_2/Ar atmosphere

Combustion and Flame 260 (2024) 113244

Contents lists available at ScienceDirect

Combustion and Flame

journal homepage: www.sciencedirect.com/journal/combustion-and-flame

Effects of oxygen enrichment on diesel spray flame soot formation in O_2/Ar atmosphere

Yu Wang [a,*], Haifeng Liu [b,*], Lei Feng [c], Noud Maes [a], Tiegang Fang [d], Yanqing Cui [b], Wentao Yi [e], Bart Somers [a], Mingfa Yao [b]

[a] Department of Mechanical Engineering, Eindhoven University of Technology, P.O. Box 513 MB, Eindhoven 5600, the Netherlands
[b] State Key Laboratory of Engines, Tianjin University, Tianjin 300072, China
[c] The 53rd Research Institute of China Electronics Technology Group Corporation, Tianjin 300308, China
[d] Department of Mechanical and Aerospace Engineering, North Carolina State University, Raleigh, NC 27695, United States
[e] Graduate School of Engineering Science, Osaka University, Toyonaka, Osaka 560-8547, Japan

ARTICLE INFO

Keywords:
Oxygen-enriched combustion
Diesel spray flames
Argon dilution
Two-color pyrometry
Soot
Two-stage Lagrangian (TSL) simulations

ABSTRACT

In this study, diesel spray combustion at oxygen-enriched conditions (oxygen volume fraction of 21–70 %) with argon dilution is experimentally investigated in a constant-volume combustion chamber. Optical diagnostics are employed to study flame development, stabilization, and soot formation at oxygen-enriched conditions. To further verify the experimental observations, two-stage Lagrangian simulations are used to analyze the effects of oxygen on the formation and oxidation of soot precursors, polycyclic aromatic hydrocarbons. Results show that replacing nitrogen in air by argon leads to a 50 % reduction of the flame lift-off length, an increased soot flame temperature by 300 K, and higher soot concentrations. Flame morphology and structure still follow the classic conventional diesel combustion model in the oxygen range of 21–40 %, while changes are observed when oxygen levels are higher than 50 %. The width and length of the soot flame are shortened, and chemiluminescence from intermediate species like CO dominates the flame natural luminosity at the spray head, where the flame temperature reaches near 3000 K. Soot reduction mechanisms at high-degree oxygen-enrichment conditions are investigated. The intrinsic mixing-limited combustion of diesel sprays leads to unavoidable fuel-rich areas locally, but the shortened flame lift-off length and sufficient oxygen supply confines soot-forming conditions to a smaller, upstream region. The residence time of fuel parcels in this confined soot-forming area is shortened due to the larger local spray velocity. Thereafter, fuel parcels enter a high-temperature fuel-lean region, where the formed soot is oxidized rapidly.

1. Introduction

In recent decades, more attention is drawn to climate change induced by greenhouse gas (GHG) emissions and public health issues caused by air pollutant emissions. As diesel engines are considered as one of the main contributions to both GHG and air pollutant emissions, the emission standards on these engines have become increasingly stringent. The European Green Deal proposed by the European Commission aims to reduce greenhouse gas emissions to net zero by 2050 [1]. As part of this proposal, the European Commission recently published a Euro 7 emission standard for combustion-engine vehicles [2]. The Euro 7 proposal consists of several measures to achieve this target, such as reducing the nitrogen oxides (NO_x) by 56 % for heavy-duty vehicles compared to Euro VI standard. Furthermore, the proposal includes that all light-duty vehicles sold in the EU will have zero CO_2 emissions from the tailpipe.

In diesel engines, the injected fuel experiences a series of complex physical and chemical events. After the discharge from a number of small orifices or nozzles, the high-velocity liquid jet breaks up into ligaments (primary breakup). This is followed by further fragmentation into small droplets (secondary breakup) caused by fluid instabilities in liquid/gas interactions. Under high-temperature, high-pressure conditions, the atomized fuel droplets are heated by the entrained air, and the evaporated fuel mixes with air to form a reactive fuel/air mixture. While turbulence and chemistry start to interact, a two-stage ignition process commences: low-temperature reactions initiate fuel decomposition into smaller hydrocarbons which are consumed in the subsequent high-temperature reactions. Provided that the fuel injection duration is

* Corresponding authors.
E-mail addresses: y.wang14@tue.nl (Y. Wang), haifengliu@tju.edu.cn (H. Liu).

https://doi.org/10.1016/j.combustflame.2023.113244
Received 23 April 2023; Received in revised form 24 November 2023; Accepted 5 December 2023
Available online 11 December 2023

Nomenclature

ASOI	after start of injection
CCDE	closed cycle diesel engine
CCUS	carbon capture, utilization, and storage
CDC	conventional diesel combustion
CO	carbon monoxide
CO_2	carbon dioxide
CVCC	constant-volume combustion chamber
ECN	engine combustion network
EGR	exhaust gas recirculation
EOI	end of injection
FWHM	full width at half maximum
GHG	greenhouse gas
LOL	lift-off length
LTC	low-temperature combustion
NL	natural luminosity
NO_x	nitrogen oxides
NTC	negative temperature coefficient
OEC	oxygen-enriched combustion
OH	hydroxyl radical
OH*	excited-state hydroxyl radical
PAHs	polycyclic aromatic hydrocarbons
PDI	probability distribution index
PSR	perfectly stirred reactor
RGB	red, green, and blue
TSL	two-stage Lagrangian
UHC	unburned hydrocarbons

long enough, the spray flame stabilizes at a well-defined location downstream of the nozzle, known as the flame lift-off length (LOL). The partially oxidized or cracked hydrocarbons travel downstream into the fuel-rich core of the spray and form polycyclic aromatic hydrocarbons (PAHs), which give rise to the formation of soot (particulate matter) further downstream. A high-temperature diffusion flame sheet in the periphery of the spray consumes most of the rich combustion products. Because of this high temperature, NO_x forms in such a diffusion flame sheet provided that nitrogen is present. All of these events of diesel spray combustion have been widely studied and described in the past decades in ambient air and diluted conditions, among others, by the Engine Combustion Network (ECN) [3].

The challenging emission standards and huge demand for clean air drives engine researchers and manufacturers to explore (near-) zero emission technologies. One of the possible solutions for achieving zero emission vehicles would be a closed cycle diesel engine (CCDE). In such a CCDE concept, after separating major combustion products of hydrocarbon fuels (i.e., CO_2 and H_2O) from the tailpipe, the remaining gases are mixed with on-board stored pure O_2 and recirculated into the intake [4,5]. Ideally, neither pollutants nor GHG are emitted since the engine is independent from the atmosphere. In practice, CCDE can be combined with modern exhaust energy recovery and carbon capture, utilization, and storage (CCUS) technologies.

In early stages of CCDE concept, the expensive cryogenic air separation was used for the oxygen production, while the CO_2 removal relied on chemical absorption by sodium hydroxide solution or phase change by compressing and cooling [6,7]. The cumbersome equipment with ultra-high cost affected the feasibility of CCDE concepts significantly, and application was limited to specific applications such as submarines [8,9]. However, in recent decades, the continuous development of CCUS and oxygen production technologies enhanced the feasibility of the CCDE concept. Benefiting from breakthroughs in advanced materials, temperature/pressure swing adsorption and membrane separation already proved to be part of important solutions for post-combustion CO_2 capture even through these technologies are still expensive and have limited capture efficiencies [10–13]. Meanwhile, the development of oxygen-selective adsorption materials also alleviates the high cost of O_2 production [14,15]. Besides, pure oxygen is also a byproduct from green hydrogen production through advanced water electrolysis [16, 17].

One of the main advantages of CCDE is that oxygen-enriched combustion (OEC) can be easily integrated due to its air-independent characteristics. By elevating the oxygen volume fraction in the intake charge, OEC can be employed as a strategy to improve engine combustion and emission performance. OEC has been investigated in several engine studies by means of adding oxygen into the intake air [18–22]. Results showed that low-degree oxygen enrichment (oxygen concentrations are generally below 30 % by volume) could significantly improve the power output and reduce carbon monoxide (CO), unburned hydrocarbons (UHC), and soot emissions. NO_x emissions, however, were increased due to the elevated flame temperature. Combining OEC with the CCDE concept, high-degree oxygen enrichment is possible since the remaining oxygen in the exhaust gases can be recirculated. Yi et al. investigated the combustion processes of diesel sprays under O_2/N_2 atmospheres with oxygen level of between 21–70 % in an optical constant-volume combustion chamber (CVCC) [23]. Results showed that at an oxygen level of 70 %, the pixel averaged soot flame temperature based on two-color pyrometry increases by over 500 K when compared to ambient air conditions. Because of the availability of oxygen, the size of the sooting flame is highly reduced. However, nitrogen dilution leads to NO_x formation in high-temperature flames, which may accumulate during closed-cycle recirculation and/or acidify the condensed water. Therefore, replacing nitrogen by carbon dioxide is considered to avoid NO_x formation [24]. Wang et al. tested diesel spray combustion in an O_2/CO_2 atmosphere with oxygen level of 50–65 % in a CVCC [25]. The high fluctuations of flame natural luminosity denoted that CO_2 dilution is prone to unstable combustion. This is in accordance with engine experiments using O_2/CO_2 by Tan and Hu., which found that a much higher oxygen concentration (>50 %) was required for stable operation of engine under CO_2 dilution cases compared with nitrogen dilution [26]. Chemical kinetic modeling showed that CO_2 contributes to a new formation reaction of OH radical [$CO+O_2+H\bullet \rightarrow CO_2+OH\bullet$], but meanwhile, the pyrolysis reaction [$CO_2 \leftrightarrows CO+1/2(O\bullet+O\bullet) \leftrightarrows CO+1/2O_2$] plays an important role over 2650 K [27]. The obstacle to CO oxidation is likely a main reason for unstable combustion and derated engine performance when using CO_2 dilution.

Argon is another feasible dilution gas to be used in CCDE to achieve nitrogen-free combustion. Argon is the third most common gas in the Earth's atmosphere (0.93 %) and its annual global production is over 700,000 ton [28]. Owing to the high heat capacity ratio (also known as the adiabatic index), adding argon into intake gas has been investigated to improve engine efficiency, especially at heavy EGR conditions [29–32]. Besides the dilution effect, the thermal and chemical effects of argon on the autoignition process of diesel surrogate fuels have been studied at low oxygen levels (around 15 %) by experiments and chemical kinetic simulations [33,34]. With its lower heat capacity (thermal effect) and higher third-body collision efficiencies (chemical effect), argon diluted gas results in a faster ignition than nitrogen, especially within the negative temperature coefficient (NTC) region. Spectral analysis of diesel spray flames at O_2/Ar atmosphere showed that at high oxygen levels (> 60 %), the natural luminosity in the flame tip is dominated by chemiluminescence, instead of soot radiation, with a peak spectral intensity at the wavelength of 450 nm [35]. This indicates that the pathway of soot formation at high oxygen levels differs from that at air conditions.

However, few studies focus on soot formation under oxygen-

enriched conditions with argon dilution. In this study, optical diagnostics and two-stage Lagrangian simulations are employed to investigate the effects of oxygen enrichment on soot formation in diesel spray flames when using an O_2/Ar atmosphere. The present work is structured as follows. Section 2 introduces the methodology of this study, including the experimental apparatus, optical diagnostic methods, numerical simulation model, and test conditions. Then, the results are analyzed and discussed in Section 3. Finally, the general conclusions are detailed in the last section.

2. Methodology

2.1. Optically accessible constant-volume combustion chamber

An optically accessible constant-volume combustion chamber is used to provide a high-temperature high-pressure environment to investigate fuel spray combustion Fig. 1 shows the schematic diagram of the experimental apparatus. The effective diameter of the transparent quartz window (JSG1 type) is 100 mm. The vessel is charged by a high-pressure gas cylinder to the setting ambient pressure. An electric heater is installed at the bottom of the vessel to heat the admitted gas to up to 850 K. Three thermocouples are installed at 10, 50, and 90 mm downstream from the injector nozzle tip to measure the vertical gradient of temperature caused by buoyancy. The temperature difference in the visible test region is less than 20 K when the set ambient temperature is 800 K. A Bosch high-pressure single-hole solenoid injector with an orifice diameter of 0.14 mm is installed at the center of the top lid. Fuel is supplied by a common rail injection system. An injection control system is used to control the fuel pressure from the pump and the energizing duration of the injector.

2.2. High-speed visualization of flame natural luminosity

A high-speed color camera (Photron FASTCAM SA5) equipped with a 50-mm lens (Nikon AF f/1.4) is used to record the flame natural luminosity (NL). The settings of the high-speed camera are as follows: aperture of f/16, frame rate of 10 kfps, and resolution of 768×768 pixels. In case of diesel flames, the NL has two main components: chemiluminescence signal from small molecules or excited radicals, and incandescence signal emitted by the hot soot particles. The latter approximately follows Plank's radiation law, and its intensity is generally several orders of magnitude higher than the chemiluminescence intensity [36,37]. The post-processing procedures of the collected high-speed RGB images are shown in Fig. 2. The time after start of injection (ASOI) for each image is labeled at the top left corner. To highlight the intensity of NL, the original RGB images are first converted to grayscale images and then rendered as falsecolor images using MATLAB. The ensemble-averaged falsecolor images from 10 injections depict the NL configuration at a specific test condition.

In addition, RGB images also contain limited spectral information. Previous studies using a high-speed color camera found that at high oxygen levels (e.g., 60 %), the soot incandescence region shrinks considerably, while a chemiluminescence-dominant region ("blue region") appears at the downstream portion of the diesel spray flames [23,35]. The single-shot RGB image in the left-most panel of Fig. 2 shows an example of this. To better understand the transformation of flame structure, a probability distribution index (PDI) is introduced. The right panel of Fig. 2 shows the camera spectral response of RGB channels and black-body spectral radiant exitance up to 4000 K. For incandescence-dominant regions in spray flames, the pixel values in RGB images generally follow $R>G>B$. However, as mentioned before, previous spectrum diagnostics denoted that the wavelength of peak spectral intensity is around 450 nm in the chemiluminescence-dominant regions [35], where the blue channel of the high-speed camera has the highest quantum efficiency. Therefore, for each RGB image, binarization is applied within the flame boundary (outlined by the 1 % of maximum intensity in the corresponding grayscale image) to define the chemiluminescence-dominant regions (set to 1 where $B>R$) and the soot-dominant regions (set to 0 for the remaining flame areas). The binarized flame images are ensemble averaged to obtain the PDI result, i.e., the likelihood that soot or chemiluminescence is present. A PDI of 0 indicates that soot is always observed at this location, while a PDI of 1 indicates the location where chemiluminescence is always dominant. It is noteworthy that this binary criterion is quite strict for

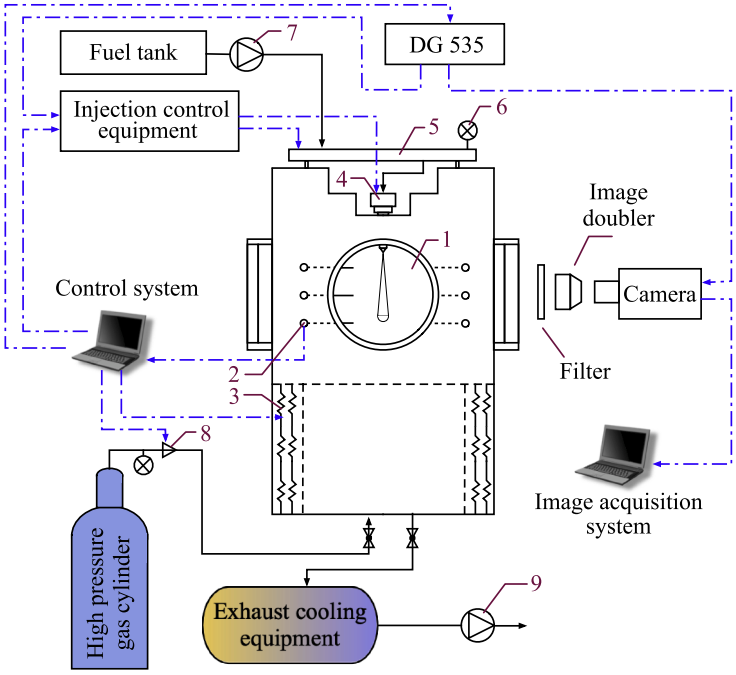

Fig. 1. Schematic diagram of the experimental setup.
1. Quartz window; 2. Temperature/pressure sensors; 3. Electric heater; 4. Injector; 5. Common rail injection system; 6. Pressure gauge; 7. Fuel pump; 8. Electromagnetic valve; 9. Vacuum pump.

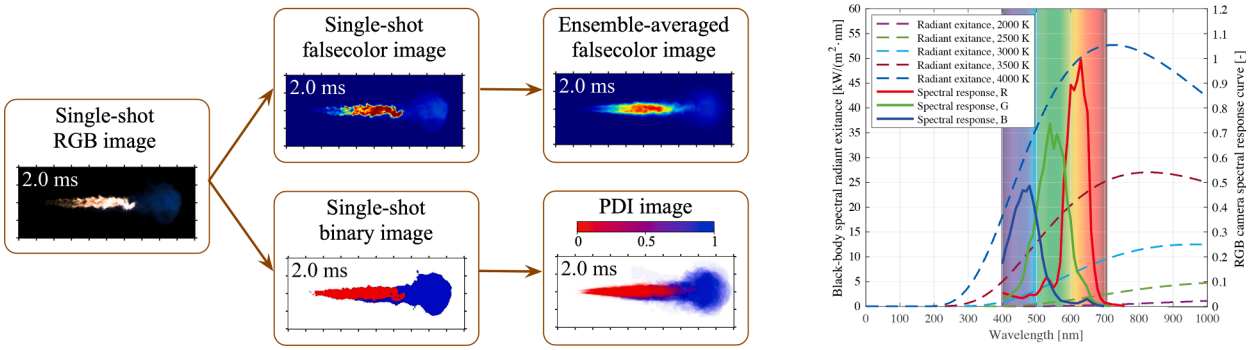

Fig. 2. Post-processing of high-speed color images. Left panel: an example of image processing procedures. Right panel: camera spectral response of RGB channels and black-body spectral radiance exitance up to 4000 K.

chemiluminescence-dominant region due to the much lower spectral response of the blue channel and the much higher intensity of soot radiation. Therefore, regions with a PDI of 1 may comprise a lot of chemiluminescence (which is overwhelmed by soot incandescence), but the regions with a PDI of 0 can be considered as anywhere from nearly to completely free of soot.

2.3. OH* chemiluminescence imaging

The hydroxyl radical (OH) is an important intermediate species in combustion reactions, which denotes the high-temperature reaction zones in diffusion flames. The chemiluminescence of excited-state hydroxyl (OH*) radicals in the $A^2\Sigma^+ - X^2\Pi$ (0,0) band can be captured by an intensified camera with spectral filters centered near 307.8 nm. The method of determining flame lift-off length from line-of-sight OH* chemiluminescence images was proposed by Higgins and Siebers [37], and it has been widely used in flame LOL studies [38–42]. In this study, the time-averaged, line-of-sight OH* chemiluminescence images are recorded using an ICCD camera (Andor DH734i-18F-03) with a bandpass filter centered at 310 nm with a FWHM of 10 nm. Diesel sprays with a long injection duration of 6.9 ms are imaged in the quasi-steady phase between 3.5 ms and 6.5 ms ASOI.

2.4. Two-color pyrometry

Two-color pyrometry is employed to measure the line-of-sight soot distribution and soot flame temperature in diesel spray flames. According to Plank's law of radiation and a gray-body approximation of soot particles, the temperature and *KL* factor can be determined by collecting the soot radiation at two different wavelengths. *K* is an absorption coefficient proportional to soot concentration, and *L* is the optical path length. The detailed derivations of two-color pyrometry can be found in previous literature [23,43–45]. In this study, the ICCD is equipped with an image doubler (VZ14–0519, LaVision) where two bandpass filters centered at 450 nm (Andover 450fs10–50, 10 nm FWHM) and 650 nm (Andover 650fs10–50, 10 nm FWHM) are installed to collect two monochromatic radiation wavelengths. The diesel sprays are imaged at quasi-steady state (4.5 ms ASOI) with an exposure time of 100 μs. To calibrate the two-color measurement, the same imaging system is used to record the radiation from a tungsten halogen light source (Ocean LS-1-LL, 2800 K lamp) where the radiation intensities at 450 and 650 nm are known. Soot flame temperature and *KL* factor are calculated by iterative algorithms for image postprocessing in MATLAB.

Two-color pyrometry has relatively large uncertainties in both soot temperature and concentration due to its intrinsic line-of-sight nature, and potentially suffers further from turbulence-induced motion blur. The non-uniformity of temperature and soot distribution in diesel sprays results in a temperature uncertainty of around 5–10 % and a *KL* uncertainty of around 50 % [43,45–47]. In this study, two-color pyrometry is used to identify the soot formation area and to provide qualitative information of temperature and soot concentration as function of different oxygen-enrichment levels in an argon environment.

2.5. Test conditions

Table 1 lists the experimental conditions of this study. Ambient temperature, ambient pressure, and injection pressure are fixed at 800 K, 40 bar, and 1000 bar, respectively. Injection durations are chosen to guarantee that the quasi-steady state of diesel spray flames is reached at all test conditions. Hence injection duration is set to 3.6 ms for high-speed visualization and to 6.9 ms for OH* chemiluminescence imaging and two-color pyrometry (the hydraulic delay is already deducted). The tested fuel is Chinese National V standard diesel. Ambient gases of O_2/Ar mixture with different oxygen volume fractions (21–70 %) are tested, and synthetic air is also tested as a reference. The absolute error of the oxygen volume percentage is controlled below 0.5 %. For each optical diagnostic technique, 10 injections are recorded to obtain ensemble-averaged images and data.

2.6. Two-stage Lagrangian simulations

A two-stage Lagrangian (TSL) model is used to better understand soot precursor formation in diesel spray flames at oxygen-enriched conditions. The TSL model was first proposed by Broadwell and Lutz to simulate combustion processes in turbulent gaseous jet flames [48]. It adopts a minimalistic turbulent entrainment model while retaining the ability to use detailed chemical kinetic mechanisms. The development of a TSL model is based on the experimental observation that in a turbulent jet diffusion flame, combustion reactions occur in two separate zones: a relatively well-mixed core region and a diffusion flame sheet at the periphery of the jet. The two stages refer to the entrained ambient gas initially mixing and reacting in the diffusion flame sheet, followed by the stage where they enter the homogeneous core region. The two-reactor configuration of the TSL model employs two perfectly stirred reactors (PSR) to simulate the homogeneous core region and the diffusion flame sheet, respectively. Later, Pickett et al. extended the applicability of the TSL two-reactor model to lifted diesel spray flames in compression ignition engines to investigate PAHs formation at EGR conditions [49]. Based on its success to capture relevant phenomena, the TSL two-reactor

Table 1
Experimental conditions.

Parameters	Values
Ambient temperature [K]	800
Ambient pressure [bar]	40
Injection pressure [bar]	1000
Oxygen volume fraction	O_2+N_2: 21 % O_2+Ar: 21, 30, 40, 50, 60, and 70 %

model has been widely used in simulating fuel spray combustion under engine-like conditions [50–52].

In the TSL simulations, a detailed chemical mechanism of n-heptane is employed to simulation diesel combustion. This chemical mechanism was proposed by Chen et al. [53]. It is composed of several well-validated submechanisms, including C0-C4, gasoline surrogates (toluene reference fuel and 1-hexene), and PAHs growth reactions up to C20 [54–56]. The TSL model is built with the open source chemical kinetic solver Cantera [57].

Fig. 3 shows the schematic diagram of the TSL model for diesel spray flames (bottom panel) with recent optical/laser diagnostic-based observations on non-reacting (top panel) and reacting (middle panel) n-dodecane sprays. These experiments on steady state diesel spray flames revealed similar observations as those on gaseous jet flames. As shown in the green regions of the middle panel of Fig. 3, the relatively homogeneous core region evolves from upstream to downstream regions: formaldehyde is first formed just before the LOL and continues to some extent beyond it (indicated by the first white bracket below the spray) [41]. Downstream from the formaldehyde structure, polycyclic aromatic hydrocarbons are formed due to the high equivalence ratio together with the high local temperature (indicated by the second white bracket). Eventually, the concentration of PAHs reduces due to the generation of soot particles. Note that this is in fact downstream of the indicated bracket in Fig. 3 where signal reduces due to the laser-sheet limits (indicated by the colored triangles). The high-temperature, near stoichiometric diffusion flame sheets are located at the jet periphery, where a large amount of OH radicals can be observed (red regions). The model traces a fuel parcel from a Lagrangian viewpoint by solving the evolution of species mass fractions and temperatures in two PSR which move along the spray axis from the nozzle exit to downstream regions.

The two reactors in the TSL model are assumed to be under constant pressure conditions. The equations for the conservation of species mass and energy for the homogeneous core reactor are as follows [48]:

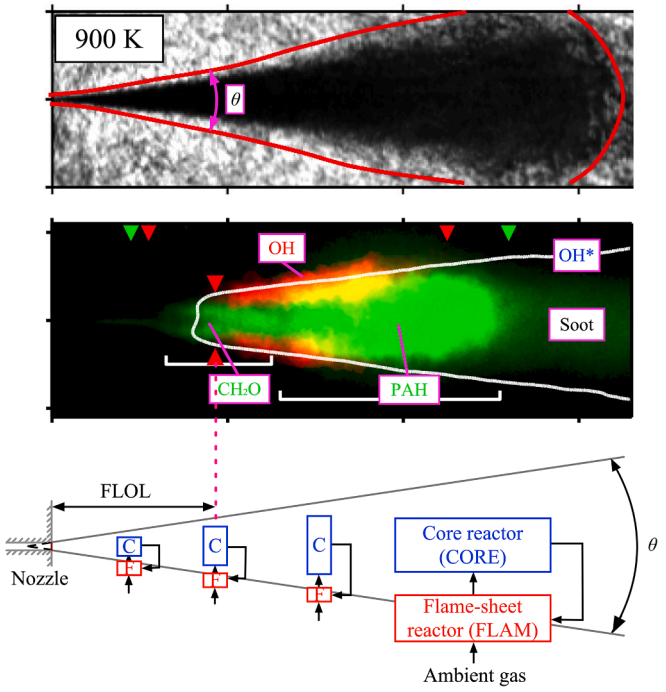

Fig. 3. TSL model for fuel spray combustion. Top: outline of ensemble averaged non-reacting n-dodecane sprays (© SAE International) [58]. Middle: ensemble averaged species distribution in a reacting n-dodecane spray from optical/laser diagnostics [41]. Bottom: schematic diagram of the two-reactor TSL model [49]. The top and middle panels are based on and reprinted with permissions.

$$\frac{dm_h}{dx} = \dot{m}_e \tag{1}$$

$$\frac{dY_{k,h}}{dx} = \frac{(1+B)}{m_h}\frac{dm_h}{dx}\left(Y_{k,f} - Y_{k,h}\right) + \left(\frac{\dot{\omega}_k W_k}{\rho}\right)_h \frac{1}{u}, \quad k = 1, \cdots, K \tag{2}$$

$$\frac{dT_h}{dx} = \frac{(1+B)}{m_h C_p}\frac{dm_h}{dx}\sum_k Y_{k,f}\left(h_{k,f} - h_{k,h}\right) - \frac{1}{\rho_h u C_p}\sum_k \left(h_k \dot{\omega}_k W_k\right)_h - \frac{\dot{q}_R}{u C_p} \tag{3}$$

where x is the axial distance from the nozzle, $\dot{m}$ is the axial mass flow rate, m is the reactor mass, Y_k is mass fraction of species k, K is the total number of species, ρ is the density, T is the temperature, c_p is the specific heat at constant pressure, and u is the average velocity in the axial direction. h_k, $\dot{\omega}_k$, and W_k are the enthalpy, molar production rate, and molecular rate of species k, respectively. Subscripts$h$, f, and ∞ denote the homogeneous core reactor, flame sheet reactor, and surroundings, respectively. The entrainment rate, $\dot{m}_e$, is a model input. $\dot{q}_R$ is the radiation loss that is neglected here for simplicity. As mentioned before, the flame-sheet reactor represents the reaction zone with its diffusive layers, which remains stoichiometric as long as the homogeneous core reactor contains a fuel-rich mixture. To mix the entrained fluid from the surroundings and homogeneous core reactor in the chemical stoichiometric proportion, the homogeneous stream is controlled by the parameter $B = (Z_{st} - Z_\infty)/(|Z_h - Z_{st}|)$, where Z is the Bilger mixture fraction.

The lift-off length is simulated through the adjustment of the initial diffusion flame. The flame-sheet reactor is initially set to a non-reacting mixture temperature. Once the LOL position is reached (LOL is an input parameter of TSL model), the flame-sheet reactor is set to its flame temperature at equilibrium state. Thereafter, it remains at steady state, delivering high-temperature combustion products into the core reactor as follows,

$$0 = \frac{1}{\tau}\left[\left(Y_{k,\infty} - Y_{k,f}\right) + B\left(Y_{k,h} - Y_{k,f}\right)\right] + \left(\frac{\dot{\omega}_k W_k}{\rho}\right)_f, \quad k = 1, \cdots, K \tag{4}$$

$$0 = \frac{1}{\tau C_p}\left[\sum_k Y_{k,\infty}\left(h_{k,\infty} - h_{k,f}\right) + B\sum_k Y_{k,h}\left(h_{k,h} - h_{k,f}\right)\right] - \frac{1}{\rho_f C_p}\sum_k \left(h_k \dot{\omega}_k W_k\right)_f - \frac{\dot{q}_R}{C_p} \tag{5}$$

The entrainment rate of ambient gas is taken from the one-dimensional spray model for high-pressure diesel sprays proposed by Musculus and Kattke [59], which requires several inputs such as the pressure and density of the fuel and ambient gases, as well as some nozzle-specific parameters. The temperature of liquid fuel is reduced to the gaseous fuel temperature in consideration of the latent heat of vaporization.

3. Results and discussion

3.1. Flame development and morphology

High-speed visualization of flame natural luminosity can provide insights into flame development and morphology at different oxygen concentrations with argon dilutions Fig. 4 shows the true-color NL images from a single injection (top panel) and the falsecolor images of ensemble-averaged NL intensity. At an oxygen level of 21 %, NL is captured by the camera at around 1.5 ms ASOI. Then the lifted flame stabilizes at a well-defined location, and a bright soot vortex head appears at the flame tip while penetrating downstream. The head of the spray flame moves beyond the visible region after 3.0 ms ASOI. Fuel injection ends at 3.6 ms, after which it takes more than 1.5 ms for the remaining fuel to burn out. With the increase of oxygen level to 40 %, the first appearance of NL is advanced, and NL intensity at the sooting

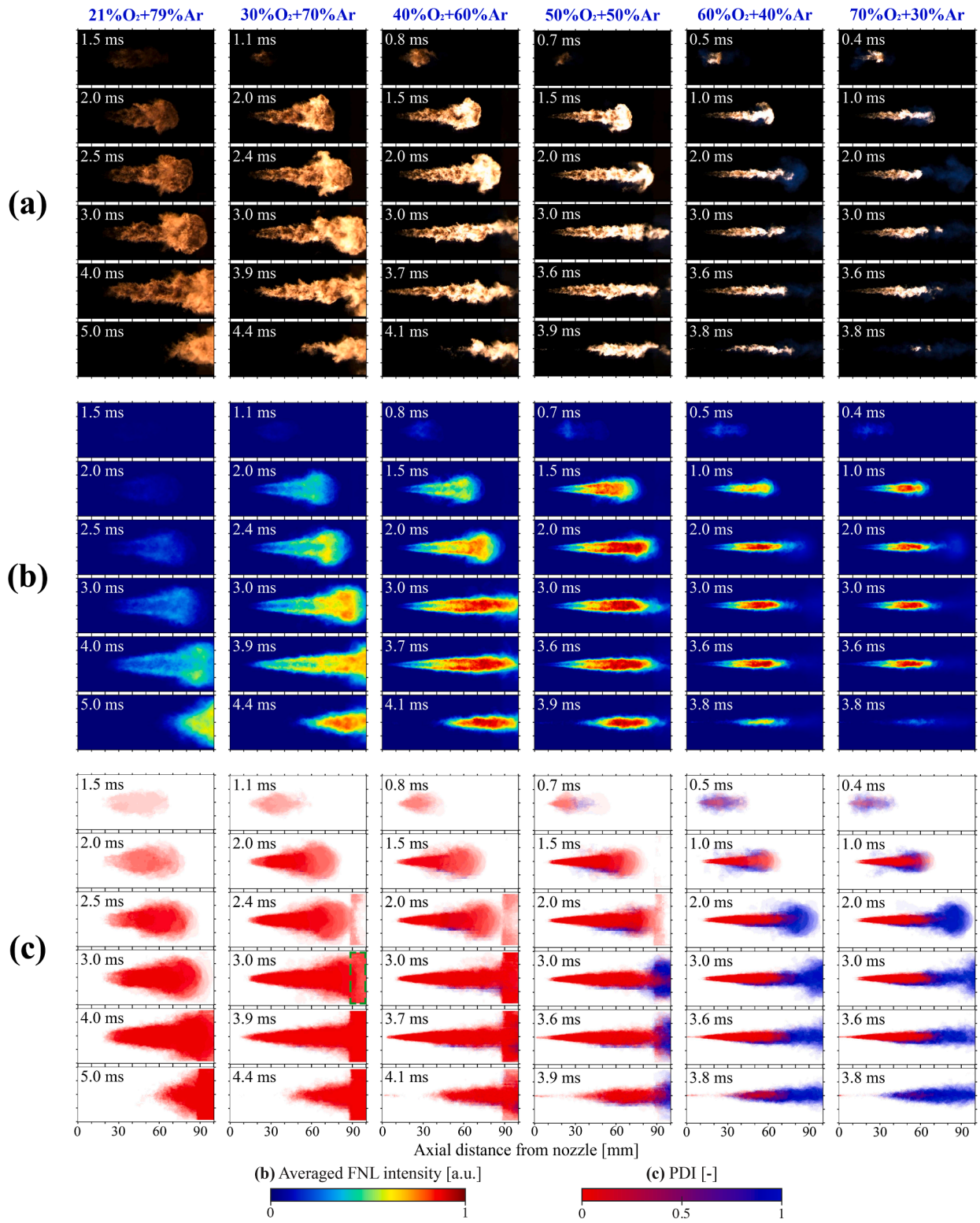

Fig. 4. Development of diesel spray flames at different oxygen enrichment levels (21–70 %) with argon dilutions. (a) Single-shot true-color NL images (the same camera settings are used in all cases). (b) Ensemble-averaged falsecolor NL images. (c) Probability distribution index (PDI) results. The dashed green box in PDI results denotes the noise region where the NL reflected by a metal wall can be detected.

head further increases. However, the single-shot and ensemble-averaged results indicate that the flame morphology and structure for the oxygen level of 21–40 % still follow the classic conventional diesel combustion (CDC) model proposed by Dec [60].

The morphology of the diesel spray flames alters pronouncedly when the oxygen level rises over 50 %. The width and length (during the quasi-steady phase) of the soot structure are shortened, and the tip of soot flame appears more erratic. It is noted that there are probably not many changes in the physical processes such as spray penetration and ambient entrainment. Chemically, however, the increased availability of oxygen

lowers equivalence ratio and promotes soot oxidization. In this case, soot may or may not form in certain regions of the jet head during the quasi-steady state. This leads to the hemisphere-like soot head wrinkling and shrinking, and the ensemble-averaged NL signal approaches a narrow belt-like shape. More interestingly, the major components of NL at the flame tip turns from soot incandescence to chemiluminescence when oxygen levels are higher than 50 %, as shown in PDI results in Fig. 4(c). During image binarization, the absolute NL intensity information is lost, while the relative intensity between image R and B channels is preserved. As mentioned in Section 2.2, regions with a PDI of 1 denote the chemiluminescence-dominated areas which are almost free of soot. It is indicated that at an oxygen level of 70 %, soot is formed at an axial distance of around 15 mm, while all soot is fully consumed during the quasi-steady state when moving downstream to around 70 mm. Hence, it seems that OEC is capable of achieving ultra-low soot generation by oxidizing the soot formed upstream in downstream high-temperature regions where sufficient oxygen is present. This will be analyzed in more detail in the section below.

A radially integrated PDI signal as a function of time (I_{xt}) is calculated to compare the transient phases of diesel spray combustion, as shown in Fig. 5. The procedure of radially integrating camera-based intensity signals is explained further in the work by Maes et al. [41]. The I_{xt} results at different oxygen levels are normalized using the maximum value for all individual cases. The axial distance in these graphs ends at 87 mm since the PDI signal comprises strong noise signal in the axial location range of 87–100 mm, where the NL is reflected by an opposite wall (as shown in the dashed green box in Fig. 4). The spray penetration (S) at different oxygen levels is calculated according to the 1-D spray model proposed by Musculus and Kattke [59] with the assumption of a steady-state injection. It shows that the effects of reduced ambient density at higher oxygen levels (since Ar is heavier than O_2) on spray penetration is minimal. It is indicated by the I_{xt} plots that the 2nd-stage ignition appears at an earlier moment and at a more upstream position with the increase in oxygen concentration. Moreover, the high-temperature chemiluminescence during the 2nd-stage ignition is intense enough to be directly captured by the high-speed camera at an oxygen level of 70 %.

With the increase in oxygen level, the duration of the burn-out phase is reduced. An obvious combustion recession phenomenon, where the lifted flame travels upstream towards the nozzle after the end of injection (EOI), can be observed with the given camera settings when oxygen percentages rise above 30 %. This phenomenon can help consume the remaining fuel and hence reduce UHC emissions [61,62]. Previous investigations showed that the entrainment of ambient gases into the spray increases by up to a factor of three after EOI, and that the region of increased entrainment travels downstream at twice the initial jet penetration rate (the so-called “entrainment wave”) [59]. The I_{xt} plots also indicate that the combustion recession at oxygen-enriched conditions is composed mostly out of soot recession and that the soot emission can reach very close to the nozzle when oxygen levels are higher than 30 %. This is because combustion recession is autoignition dominated [61], while the ignition delay is significantly shortened by the increased oxygen concentrations. After EOI, fuel autoignites rapidly near the nozzle regions where a rich mixture is formed due to mixing-limited vaporization, leading to soot recession. However, halfway along the length of the spray flame (e.g., 40 – 60 mm from the nozzle for an oxygen percentage of 70 %) where NL is dominated by soot radiation at quasi-steady state conditions, the NL is dominated by chemiluminescence during the burn-out phase because of the increased entrainment after EOI. This means that the soot formed during the steady-state and combustion recession processes can be effectively oxidized during the burn-out phase after EOI.

3.2. Flame stabilization and soot formation

Soot formation and oxidation processes at oxygen-enriched conditions are of great interest for further investigation since the reduced sooting region in a diesel spray head is an interesting phenomenon which is only reported in a limited amount of studies [23,35]. Fig. 6 shows the single-shot soot flame temperature and ensemble-averaged soot *KL* factor results based on two-color pyrometry measurement at quasi-steady state, as well as the equivalence ratio contour from the 1-D spray model [59] and PDI from high-speed NL visualization. Note that representative single shot temperature results are shown to minimize effects of averaging on the minimum and maximum temperatures encountered in the flames. The flame lift-off length, as a key parameter for flame stabilization which plays an important role in soot formation, is marked by green triangles in the different panels. Note that the LOL results are also shown in Appendix Fig. A.1.

In the normal air conditions, the diesel spray flame stabilizes at an axial location of around 34 mm where the equivalence ratio at centerline ($\Phi_{centerline}$) is above 4, and soot can be observed starting from 50 mm. Due to the limited optically accessible region, only part of the soot flame is visible, where the soot temperature is basically in a range of 2000–2300 K with a moderate *KL* factor value (a soot head with large *KL* factor is expected to persist beyond the visible region). Through replacing nitrogen by argon, however, the LOL is almost halved, and flame temperatures increase to over 2600 K, accompanied by an immense increase in *KL*. The change is mainly due to the much lower heat capacity of argon when compared to nitrogen. In addition, according to the Φ contour predicted by the 1-D spray model, the higher density of argon results in a slightly higher local equivalence ratio compared to air. In Appendix Fig. A.2, the adiabatic flame temperature (T_{ad}) versus equivalence ratio is calculated for different ambient gases.

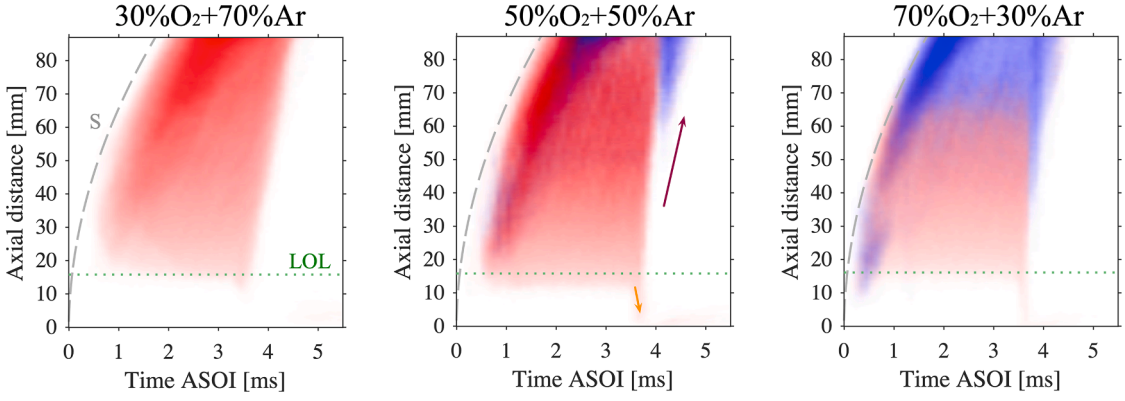

Fig. 5. Radially integrated PDI signal at different oxygen enrichment levels with argon dilution as a function of axial distance and time (I_{xt}). Bilinear interpolation is used to enhance image resolution. Dashed gray lines show the spray penetration (S) predicted by a 1-D spray model [59]. Dotted green lines show the flame lift-off length. In the middle panel, the orange arrow denotes combustion recession after the end of injection, and the brown arrow denotes the burn-out process.

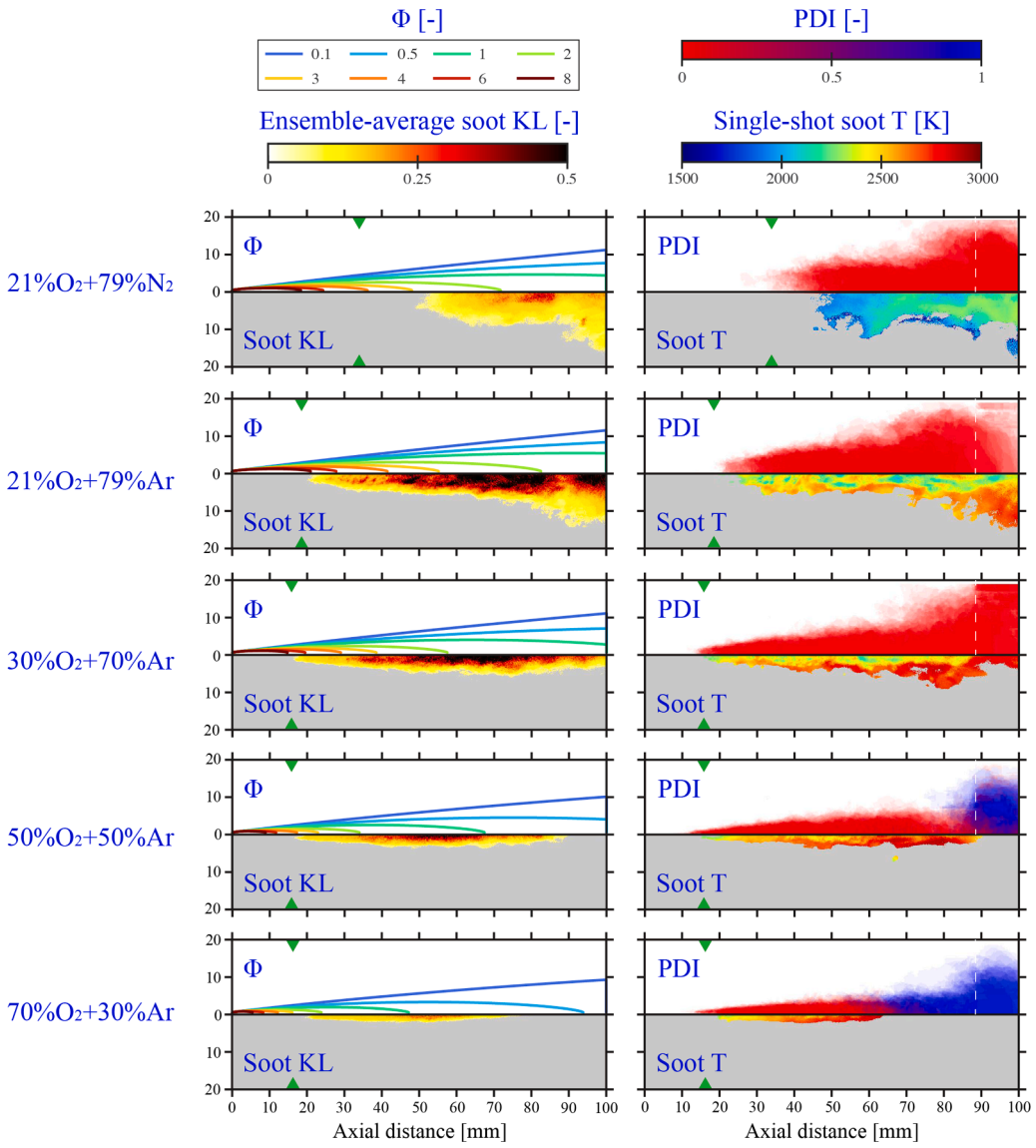

Fig. 6. Soot KL and temperature results at different oxygen enrichment levels with argon dilution. At each condition, the predicted equivalence ratio (top left), ensemble-averaged soot *KL* (bottom left), PDI (top right), and single-shot soot temperature (bottom right) are presented. The green triangles indicate the flame lift-off length.

T_{ad} at stoichiometric condition increases from 2607 K to 2950 K when replacing nitrogen in air by argon. The thermal effect of argon promotes temperature increase from the accumulation of local heat release. Hence, the flame is able to stabilize at a location much closer to nozzle. However, the shortened LOL means the fuel-ambient mixture burning at a very rich condition ($\Phi_{centerline}$ at the LOL is predicted to reach a value of 8, as shown in the top panel of Fig. 7). Consequently, the dense soot cloud can be detected in the entire spray core region.

With the increase of oxygen level to 30 %, more entrained oxygen reduces local equivalence ratio while the LOL is only slightly reduced, leading to a lower $\Phi_{centerline}$ at the LOL position. Therefore, the width of the highly sooting region narrows, and the soot head shrinks. When oxygen percentages reach 50 %, the soot head totally diminishes, and the soot temperature at the soot flame tip reaches values close to 3000 K. At the farthest downstream part of the spray, there is still a hemispherical head due to the reduced axial velocity and expansion of high-temperature gases. However, as shown in the PDI subpanel, soot incandescence in this spray head is replaced by strong chemiluminescence from intermediate species at local temperatures that approach 3000 K. At the oxygen level of 70 %, the soot region shrinks further to a narrow belt-like shape in the axial location range of 20–70 mm, with a much lower *KL* factor.

To better understand the effects of oxygen enrichment on soot formation and consumption in diesel spray flames, soot precursors (polycyclic aromatic hydrocarbons) are investigated using the two-stage Lagrangian model. Fig. 7 shows the equivalence ratio, pyrene (A4) yield, and CO yield, respectively, in the homogeneous core reactor for different ambient gases. As mentioned before, the tested ambient gas components just have a minimal influence on spray penetration. Hence, the top x-axis in the upper panel shows the time required for the spray at 70 %O_2+30 %Ar conditions to arrive at certain distances. The A4 and CO yields are defined by the shares of total carbon atoms taken by these two species. At the normal air condition, around 4 % of carbon atoms convert into pyrene at an axial location of 70 mm. The maximum A4 yield increases to over 10 % when replacing nitrogen with argon. This indicates that more soot is formed, substantiating the two-color pyrometry results. With the increase in oxygen concentration, the maximum A4 yield is reduced, and its location moves upstream. At the highest oxygen level of 70 %, the peak A4 yield is less than 100 ppm. An interesting observation is that centerline equivalence ratios at the LOL are quite close for air and

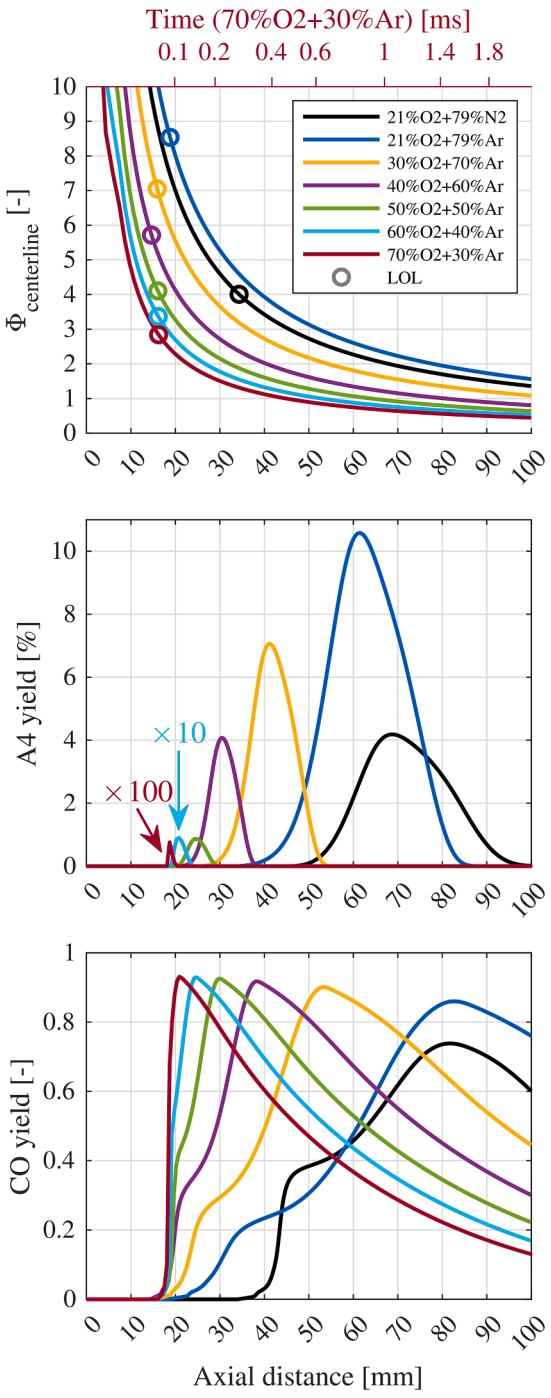

Fig. 7. Results of TSL simulations versus axial distance at different oxygen enrichment levels: equivalence ratio at the spray centerline (top panel), A4 yield (center panel), and CO yield (bottom panel). The LOL is denoted by circle markers in the top panel. In the top panel, the x-axis above the graph shows the time for a spray at 70 %O_2+30 %Ar conditions to reach the axial distances on the lower x-axis. In center panel, A4 yield for 70 %O_2+30 %Ar is magnified by 100 times.

50 %O_2+50 %Ar conditions (Φ≈4), but the latter has a much lower A4 yield. The reason is believed to be the short residence time in the fuel-rich regions. As shown in the time axis, the $\Phi_{centerline}$ at 50 %O_2+50 %Ar condition drops from 4 to 2 within 0.2 ms, while it takes more than 0.6 ms at the normal air conditions.

To address the importance of residence time, the Φ-T trajectories of the homogeneous core reactor are presented in Fig. 8 with the markers

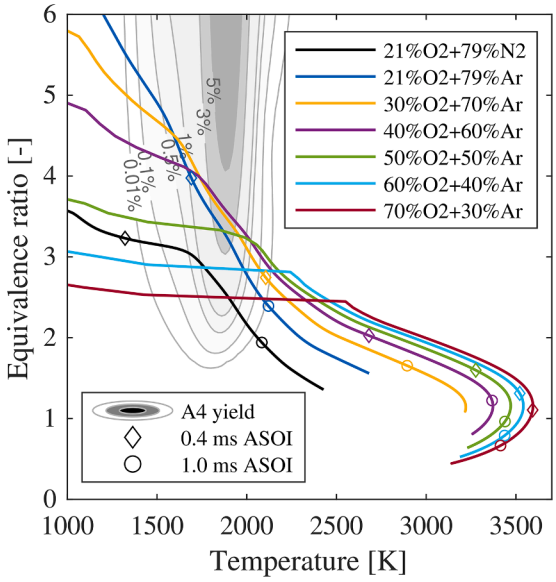

Fig. 8. TSL simulation results in *ϕ-T* coordinates. The filled contour indicates the A4 yield from closed-reactor simulations of heptane (at constant-pressure, without solving the energy equation, using a residence time of 1.0 ms). Two moments in time (0.4 and 1.0 ms ASOI) for each condition are shown by markers.

showing the dwell time between 0.4 and 1.4 ms ASOI. A filled contour of A4 yield is also presented in the background, which is determined from the kinetic modeling in closed reactors using the same chemical mechanism with a residence time of 1.0 ms, similar to the work by Kitamura et al. [63]. Since the energy equation is not solved, ambient gas components only have a minimal influence on the "pyrene islands," as shown in Appendix Fig. A.3. Therefore, the pyrene island as calculated for the 70 %O_2+30 %Ar condition is used in Fig. 8. Pyrene is prone to be formed in fuel-rich regions with temperatures between 1400 and 2200 K.

In TSL modeling, a fuel parcel flowing from the nozzle to a downstream region is traced. As shown in Fig. 8, all Φ-T trajectories at the tested conditions pass through the pyrene island. However, the traced fuel parcel has a relatively long residence time of over 0.5 ms in the pyrene island at the oxygen levels of 21 % (for both argon and nitrogen dilutions), which accounts for the observed higher soot *KL* factors at these conditions. When oxygen percentage is higher than 50 %, on one hand, the Φ-T trajectories pass through pyrene island at a lower equivalence ratio in a near horizontal way (meaning that the temperature increases sharply when fuel parcel moves to LOL location). On the other hand, the traced fuel parcel stays at a high-temperature (> 3000 K) condition with equivalence ratio below 2 for a long duration (between 0.4 and 1.0 ms ASOI). It is noteworthy that the temperature is over-predicted due to the lack of heat transfer (radiation loss) model. However, it is known from soot temperature results in Fig. 6 that soot temperatures reach above 2600 K at 0.4 ms ASOI (corresponding to the axial location of 42 mm). Therefore, the short residence time in the soot island accounts for the lower soot concentration at high oxygen level conditions, while the long residence time in high-temperature fuel-lean region accounts for the enhanced soot oxidation which finally leads to the shortened and narrowed soot area.

Carbon monoxide is an important intermediate species in the combustion reaction of hydrocarbons. According to the kinetic modeling in closed reactors, CO mainly stems from fuel-rich mixtures at high-temperature conditions [64,65]. This is also substantiated by the TSL simulations as shown in Fig. 7. However, it is noted that at the 70 % O2+30 %Ar condition, CO still takes up a large fraction of total carbon atoms in downstream regions even though the $\Phi_{centerline}$ decreases below 1 starting from an axial location of 45 mm. As evidenced by

previous kinetic modeling, this is because the pyrolysis reaction of CO_2 [$CO_2 \leftrightarrows CO+1/2(O\bullet+O\bullet) \leftrightarrows CO+1/2O_2$] plays an important role at high temperatures (over 2650 K) [27]. This is also supported by previous spectroscopic analysis of flame natural luminosity, where the "blue region" at the flame tip for oxygen levels of 70 % has a strong continuous emission spectrum with a peak at near 450 nm [35]. This is consistent with the flame spectrum of CO burning in an air or oxygen ambient, consisting of a faint banded spectrum superposed on a strong continuous background which extends through the visible and near ultraviolet, with the highest intensity in the region between 350 and 450 nm [66]. Due to the abundant oxygen supply, the formed CO is expected to be consumed in the downstream region with lower local temperatures, where the chemical equilibrium of CO_2 pyrolysis reaction moves toward converting CO into CO_2.

Based on the above discussion, oxygen-enriched combustion with argon dilution shows good potential to realize ultra-low soot emissions. Moreover, the lack of in-cylinder nitrogen avoids NO_x formation. High-degree OEC as well as argon dilution makes the lifted spray flame stabilize at an upstream location. Thereby, the intrinsic mixing-limited combustion makes fuel-rich combustion unavoidable, but the reduced LOL and sufficient oxygen supply in downstream region confine soot-forming conditions to a smaller, upstream region. Fuel parcels leave the nozzle with a high axial velocity (over 500 m/s) and the axial velocity is approximately inversely proportional to axial location [59]. The high axial velocity at the LOL location results in fuel parcels having a short residence time under the soot-forming conditions. Then, they enter a high-temperature fuel-lean region, where the formed soot is quickly oxidized. The soot reduction mechanism at high-degree OEC condition is different from the well-known and well-explored low-temperature combustion (LTC) conditions, which generally prolong both ignition delay and LOL to reduce local equivalence ratio in the combustion zone. At high-degree OEC conditions, the combustion event is directly controlled by injection timing, which simplifies engine control strategies. Moreover, engine-out emissions are expected to be near zero at high-OEC conditions with argon dilutions. However, the closed cycle diesel engine layout needs to be implemented to utilize the excess oxygen and to recycle argon, which is still a huge challenge currently.

4. Conclusions

In this study, diesel spray combustion at oxygen-enriched conditions (oxygen volume fractions of 21–70 %) with argon dilution is experimentally investigated in a constant-volume combustion chamber at an ambient temperature of 800 K, ambient pressure of 40 bar, and injection pressure of 1000 bar. Optical diagnostics are employed to study flame development, morphology, and soot formation. Two-stage Lagrangian simulations are used to analyze the effects of oxygen concentration on the formation and consumption of soot precursors. The main findings from this study are listed below.

(1) At an oxygen volume fraction of 21 %, the replacement of nitrogen by argon results in an almost halved flame lift-off length, an increased soot flame temperature by 300 K, and higher soot concentration. Flame temperature and flame natural luminosity at the sooting head of the jet further increase with the increase of oxygen level to 40 %, while the flame morphology and structure still follow the classic conventional diesel combustion model.
(2) When oxygen levels rise over 50 %, the morphology of diesel spray flames alters. The hemisphere-like soot head shows more wrinkles and shrinks while the width and length of the soot flame are reduced, making the ensemble-averaged flame natural luminosity signal approach a narrow belt-like shape. Instead of soot incandescence, chemiluminescence from intermediate species like CO, dominate the flame natural luminosity at the spray head where the flame temperature reaches near 3000 K.
(3) Results from optical diagnostics and TSL simulations address that soot formation can be alleviated by shortening the residence time for fuel parcels under soot-favoring conditions. High-degree oxygen-enriched combustion with argon dilution makes the lifted spray flame stabilize closer to the nozzle when compared to diesel flames in an ambient environment consisting of plain air. The intrinsic mixing-limited combustion leads to unavoidable fuel-rich combustion, but the shortened LOL and sufficient oxygen supply confines soot-forming conditions to a smaller, upstream region. In this confined soot-forming area, the residence time of fuel parcels is shortened due to the much larger local spray velocity. Thereafter, fuel parcels enter a high-temperature fuel-lean region, where the formed soot is oxidized rapidly.

Novelty and significant statement

The combination of a closed cycle diesel engine coupled with oxygen-enriched combustion and argon dilution has potential to achieve both high efficiency and (near-) zero emissions. This study investigates the influences of oxygen enrichment and argon dilution on diesel spray flames through optical diagnostics and two-stage Lagrangian simulations. Observations in this study validate that the different soot formation and oxidation trajectory results in the change of flame morphology at high-degree oxygen-enrichment conditions. Soot reduction mechanisms at high-degree oxygen-enrichment are revealed for the first time, which addresses the importance of a reduced residence time at soot-forming conditions.

CRediT authorship contribution statement

Yu Wang: Conceptualization, Methodology, Investigation, Formal analysis, Writing – original draft. **Haifeng Liu:** Conceptualization, Supervision, Writing – review & editing. **Lei Feng:** Methodology, Investigation, Formal analysis. **Noud Maes:** Supervision, Writing – review & editing. **Tiegang Fang:** Methodology, Writing – review & editing. **Yanqing Cui:** Methodology, Investigation. **Wentao Yi:** Methodology, Investigation. **Bart Somers:** Funding acquisition, Supervision, Writing – review & editing. **Mingfa Yao:** Funding acquisition, Supervision, Writing – review & editing.

Declaration of Competing Interest

The authors declare that they have no known competing financial interests or personal relationships that could have appeared to influence the work reported in this paper.

Acknowledgments

The experimental work is supported by the National Natural Science Foundation of China (NSFC) through the Project of 51921004. The simulation work is supported by the European Union's Horizon 2020 Research and Innovation programme (SmartCHP project, Grant Agreement No. 815259).

Supplementary materials

Supplementary material associated with this article can be found, in the online version, at doi:10.1016/j.combustflame.2023.113244.

References

[1] European Commission. The European Green Deal (2019).
[2] European Commission. Proposal for a Regulation of the European Parliament and of the council on type-approval of motor vehicles and engines and of systems, components and separate technical units intended for such vehicles, with respect to their emissions and battery durability (Euro 7) and repealing Regulations (EC) No 715/2007 and (EC) No 595/2009 (2022).
[3] Engine combustion network, https://ecn.sandia.gov/ (accessed January 9, 2023).
[4] R. Shaw, H. Oman, Non-air working fluids for closed-cycle diesel engines, Proc., Intersoc. Energy Convers. Eng. Conf. (1983) CONF830812.
[5] H.W. Wu, Z.Y. Wu, J.Y. Yang, R.H. Wang, W.H. Lin, Combustion characteristics of a closed cycle diesel engine with different intake gas contents, Appl. Therm. Eng. 29 (2009) 848–858.
[6] H.W. Wu, C.T. Shu, Effects of operating parameters on steady and transient behaviors of a closed cycle diesel engine, Energy Convers. Manag. 47 (2006) 2070–2080.
[7] M. Yoo, S.J. Han, J.H. Wee, Carbon dioxide capture capacity of sodium hydroxide aqueous solution, J. Environ. Manag. 114 (2013) 512–519.
[8] G.T. Reader, I.J. Potter, J.G. Hawley, Underwater heat engines-state of the art, Am. Soc. Mech. Eng. (1992), 92 Emerg. Energy Sources Technol. Conf.
[9] G.T. Reader, J. Potter, J.G. Hawley, The evolution of AUV power systems, Ocean. MTS IEEE 1 (2002) 191–198. IEEE.
[10] N. Hedin, L. Andersson, L. Bergström, J. Yan, Adsorbents for the post-combustion capture of CO_2 using rapid temperature swing or vacuum swing adsorption, Appl. Energy 104 (2013) 418–433.
[11] S. Li, X. Yuan, S. Deng, L. Zhao, K.B. Lee, A review on biomass-derived CO2 adsorption capture: adsorbent, adsorber, adsorption, and advice, Renew. Sustain. Energy Rev. 152 (2021), 111708.
[12] M. Kárászová, B. Zach, Z. Petrusová, V. Červenka, M. Bobák, M. Šyc, P. Izák, Post-combustion carbon capture by membrane separation, Review. Sep. Purif. Technol. 238 (2020), 116448.
[13] K. Sumida, D.L. Rogow, J.A. Mason, T.M. Mcdonald, E.D. Bloch, Z.R. Herm, T. H. Bae, J.R. Long, Carbon dioxide capture in metalàorganic frameworks, Chem. Rev. 112 (2012) 724–781.
[14] S.M. Hashim, A.R. Mohamed, S. Bhatia, Current status of ceramic-based membranes for oxygen separation from air, Adv. Colloid Interface Sci. 160 (2010) 88–100.
[15] W. Zhang, D. Banerjee, J. Liu, H.T. Schaef, J.V. Crum, C.A. Fernandez, R. K. Kukkadapu, Z. Nie, S.K. Nune, R.K. Motkuri, K.W. Chapman, M.H. Engelhard, J. C. Hayes, K.L. Silvers, R. Krishna, B.P. Mcgrail, J. Liu, P.K. Thallapally, Redox-active metal–organic composites for highly selective oxygen separation applications, Adv. Mater. 28 (2016) 3572–3577.
[16] R.N. Singh, D. Mishra, A.S.K.S. Anindita, A. Singh, Novel electrocatalysts for generating oxygen from alkaline water electrolysis, Electrochem. Commun. 9 (2007) 1369–1373.
[17] M. Yu, E. Budiyanto, H. Tüysüz, Principles of water electrolysis and recent progress in cobalt-, nickel-, and iron-based oxides for the oxygen evolution reaction, Angew. Chem. Int. Ed. 61 (2022), e202103824.
[18] C.D. Rakopoulos, D.T. Hountalas, T.C. Zannis, Y.A. Levendis, Operational and environmental evaluation of diesel engines burning oxygen-enriched intake air or oxygen-enriched fuels: a review, SAE Tech. Pap. (2004), 2004-01–2924.
[19] J. Song, V. Zello, A.L. Boehman, F.J. Waller, Comparison of the impact of intake oxygen enrichment and fuel oxygenation on diesel combustion and emissions, Energy Fuels 18 (2004) 1282–1290.
[20] D.N. Assanis, R.B. Poola, R. Sekar, G.R. Cataldi, Study of using oxygen-enriched combustion air for locomotive diesel engines, J. Eng. Gas Turbines Power 123 (2001) 157–166.
[21] Y. Liang, G. Shu, H. Wei, W. Zhang, Effect of oxygen enriched combustion and water-diesel emulsion on the performance and emissions of turbocharged diesel engine, Energy Convers. Manag. 73 (2013) 69–77.
[22] P. Baskar, A. Senthilkumar, Effects of oxygen enriched combustion on pollution and performance characteristics of a diesel engine, Eng. Sci. Technol. Int. J. 19 (2016) 438–443.
[23] W. Yi, H. Liu, L. Feng, Y. Wang, Y. Cui, W. Liu, M. Yao, Multiple optical diagnostics on effects of fuel properties on spray flames under oxygen-enriched conditions, Fuel 291 (2021), 120129.
[24] Q. Tan, Y. Hu, Z. Tan, Study on diesel low-nitrogen or nitrogen-free combustion performance in constant volume combustion vessels and contributory, Atmosphere 12 (2021) (Basel).
[25] L. Wang, Y. Liu, G. Bi, L. Zhang, J. Song, A phenomenological model of diesel combustion characteristics under CO_2/O_2 atmosphere, Fuel Process. Technol. 229 (2022), 107167.
[26] Q. Tan, Y. Hu, A study on the combustion and emission performance of diesel engines under different proportions of O_2 & N_2 & CO_2, Appl. Therm. Eng. 108 (2016) 508–515.
[27] Y. Liu, L. Wang, G. Bi, P. Wei, X. He, S. Yao, J. Song, H. Sun, Analysis of the combustion mechanism of diesel surrogate fuel under CO_2/O_2 atmosphere, Fuel 309 (2022).
[28] J. Emsley, Nature's Building blocks: an A-Z Guide to the Elements, Oxford University Press, 2011.
[29] T. Li, H. Izumi, T. Shudo, H. Ogawa, Y. Okabe, Characterization of low temperature diesel combustion with various dilution gases, SAE Tech. Pap. (2007), 2007-01–0126.
[30] K. Prashanth, A. Shaik, T. Srinivasa Rao, B. Pavan Bharadwaja, Experimental investigation of argon gas induction on diesel engine performance and emission characteristics: a comprehensive study on de-NOx techniques, Process Saf. Environ. Prot. 152 (2021) 471–481.
[31] J. Huo, Y. Guan, M. Zhang, D. Zhang, J. Lyu, Z. Huang, D. Han, Diesel spray auto-ignition in different oxidizing atmospheres, Fuel 328 (2022), 125308.
[32] W. Li, Z. Liu, Z. Wang, H. Dou, Experimental and theoretical analysis of effects of atomic, diatomic and polyatomic inert gases in air and EGR on mixture properties, combustion, thermal efficiency and NOx emissions of a pilot-ignited NG engine, Energy Convers. Manag. 105 (2015) 1082–1095.
[33] S.W. Wagnon, M.S. Wooldridge, Effects of buffer gas composition on autoignition, Combust. Flame 161 (2014) 898–907.
[34] H. Di, X. He, P. Zhang, Z. Wang, M.S. Wooldridge, C.K. Law, C. Wang, S. Shuai, J. Wang, Effects of buffer gas composition on low temperature ignition of iso-octane and n-heptane, Combust. Flame 161 (2014) 2531–2538.
[35] Y. Wang, L. Feng, C. Geng, B. Chen, H. Liu, M. Yao, Natural flame luminosity and emission spectra of diesel spray flame under oxygen-enriched condition in an optical constant volume vessel, SAE Tech. Pap. (2018), 2018-01–1781.
[36] J.E. Dec, C. Espey, Chemiluminescence imaging of autoignition in a DI diesel engine, SAE Trans. (1998) 2230–2254.
[37] B. Higgins, D. Siebers, Measurement of the flame lift-off location on DI diesel sprays using OH chemiluminescence, SAE Trans. (2001) 739–753.
[38] D. Siebers, B. Higgins, Flame lift-off on direct-injection diesel sprays under quiescent conditions, SAE Trans. (2001) 400–421.
[39] D. Siebers, B. Higgins, L. Pickett, Flame lift-off on direct-injection diesel fuel jets: oxygen concentration effects, SAE Trans. (2002) 1490–1509.
[40] M.P.B. Musculus, Effects of the in-cylinder environment on diffusion flame lift-off in a DI diesel engine, SAE Trans. (2003) 314–337.
[41] N. Maes, M. Meijer, N. Dam, B. Somers, H.B. Toda, G. Bruneaux, S.A. Skeen, L. M. Pickett, J. Manin, Characterization of spray a flame structure for parametric variations in ECN constant-volume vessels using chemiluminescence and laser-induced fluorescence, Combust. Flame 174 (2016) 138–151.
[42] N. Maes, N. Dam, B. Somers, T. Lucchini, G. D'Errico, G. Hardy, Heavy-duty diesel engine spray combustion processes: experiments and numerical simulations, SAE Tech. Pap. (2018), 2018-01–1689.
[43] M.P.B. Musculus, S. Singh, R.D. Reitz, Gradient effects on two-color soot optical pyrometry in a heavy-duty DI diesel engine, Combust. Flame 153 (2008) 216–227.
[44] C. Ming, I.M.R. Fattah, Q.N. Chan, P.X. Pham, P.R. Medwell, S. Kook, G.H. Yeoh, E. R. Hawkes, A.R. Masri, Combustion characterization of waste cooking oil and canola oil based biodiesels under simulated engine conditions, Fuel 224 (2018) 167–177.
[45] K.I. Svensson, A.J. Mackrory, M.J. Richards, D.R. Tree, Calibration of an RGB, CCD camera and interpretation of its two-color images for KL and temperature, SAE Tech. Pap. (2005), 2005-01–0648.
[46] D.R. Tree, K.I. Svensson, Soot processes in compression ignition engines, Prog. Energy Combust. Sci. 33 (2007) 272–309.
[47] J. Zhang, W. Jing, W.L. Roberts, T. Fang, Soot temperature and KL factor for biodiesel and diesel spray combustion in a constant volume combustion chamber, Appl. Energy 107 (2013) 52–65.
[48] J.E. Broadwell, A.E. Lutz, A turbulent jet chemical reaction model: nO(x) production in jet flames, Combust. Flame 114 (1998) 319–335.
[49] L.M. Pickett, J.A. Caton, M.P.B. Musculus, A.E. Lutz, Evaluation of the equivalence ratio-temperature region of diesel soot precursor formation using a two-stage Lagrangian model, Int. J. Engine Res. 7 (2006) 349–370.
[50] M. Meijer, B. Somers, J. Johnson, J. Naber, S.Y. Lee, L.M.C. Malbec, G. Bruneaux, L. M. Pickett, M. Bardi, R. Payri, Engine combustion network (ECN): characterization and comparison of boundary conditions for different combustion vessels, At. Sprays 22 (2012).
[51] A. Alfazazi, O.A. Kuti, N. Naser, S.H. Chung, S.M. Sarathy, Two-stage Lagrangian modeling of ignition processes in ignition quality tester and constant volume combustion chambers, Fuel 185 (2016) 589–598.
[52] M.S. Johnson, M.R. Nimlos, E. Ninnemann, A. Laich, G.M. Fioroni, D. Kang, L. Bu, D. Ranasinghe, S. Khanniche, S.S. Goldsborough, Oxidation and pyrolysis of methyl propyl ether, Int. J. Chem. Kinet. 53 (2021) 915–938.
[53] B. Chen, X. Liu, H. Liu, H. Wang, D.C. Kyritsis, M. Yao, Soot reduction effects of the addition of four butanol isomers on partially premixed flames of diesel surrogates, Combust. Flame 177 (2017) 123–136.
[54] S.M. Sarathy, S. Vranckx, K. Yasunaga, M. Mehl, P. Oßwald, W.K. Metcalfe, C. K. Westbrook, W.J. Pitz, K. Kohse-Höinghaus, R.X. Fernandes, A comprehensive

chemical kinetic combustion model for the four butanol isomers, Combust. Flame 159 (2012) 2028–2055.
[55] M. Mehl, J.Y. Chen, W.J. Pitz, S.M. Sarathy, C.K. Westbrook, An approach for formulating surrogates for gasoline with application toward a reduced surrogate mechanism for CFD engine modeling, Energy Fuels 25 (2011) 5215–5223.
[56] N.A. Slavinskaya, U. Riedel, S.B. Dworkin, M.J. Thomson, Detailed numerical modeling of PAH formation and growth in non-premixed ethylene and ethane flames, Combust. Flame 159 (2012) 979–995.
[57] D.G. Goodwin, H.K. Moffat, I. Schoegl, R.L. Speth, B.W.Weber. Cantera. An Object-oriented Software Toolkit for Chemical Kinetics, Thermodynamics, and Transport Processes, Zenodo, 2022, https://doi.org/10.5281/zenodo.742000.
[58] N. Maes, N. Dam, B. Somers, T. Lucchini, G. D'Errico, G. Hardy, Experimental and numerical analyses of liquid and spray penetration under heavy-duty diesel engine conditions, SAE Int. J. Fuels Lubr. 9 (2016) 108–124.
[59] M.P.B. Musculus, K. Kattke, Entrainment waves in diesel jets, SAE Int. J. Engines 2 (2009) 1170–1193.
[60] J.E. Dec, A conceptual model of DI diesel combustion based on laser-sheet imaging, SAE Tech. Pap. (1997), 970873.
[61] B.W. Knox, C.L. Genzale, Scaling combustion recession after end of injection in diesel sprays, Combust. Flame 177 (2017) 24–36.
[62] D. Jarrahbashi, S. Kim, B.W. Knox, C.L. Genzale, Computational analysis of end-of-injection transients and combustion recession, Int. J. Engine Res. 18 (2017) 1088–1110.
[63] T. Kitamura, T. Ito, J. Senda, Mechanism of smokeless diesel combustion with oxygenated fuels based on the dependence of the equivalence ration and temperature on soot particle formation, Int. J. Engine Res. 3 (2002) 223–248.
[64] D. Kim, I. Ekoto, W.F. Colban, P.C. Miles, In-cylinder CO and UHC imaging in a light-duty diesel engine during PPCI low-temperature combustion, Int. J. Fuels Lubr. 1 (2009) 933–956.
[65] A. Paykani, A.H. Kakaee, P. Rahnama, R.D. Reitz, Progress and recent trends in reactivity-controlled compression ignition engines, Int. J. Engine Res. 17 (2016) 481–524.
[66] A.G. Gaydon, The flame spectrum of carbon monoxide, Proc. R. Soc. London. Ser. A. Math. Phys. Sci. 176 (1940) 505–521.